# Amino Acid Position-specific Contributions to Amyloid β-Protein Oligomerization[*][S]

**Samir K. Maji[‡1], Rachel R. Ogorzalek Loo[§¶], Mohammed Inayathullah[‡], Sean M. Spring[‡], Sabrina S. Vollers[‡2], Margaret M. Condron[‡], Gal Bitan[‡¶‖], Joseph A. Loo[§¶**], and David B. Teplow[‡¶‖3]**

*From the ‡Department of Neurology and §Department of Biological Chemistry, David Geffen School of Medicine, ¶Molecular Biology Institute, ‖Brain Research Institute, and **Department of Chemistry and Biochemistry, UCLA, Los Angeles, California 90095*

**Understanding the structural and assembly dynamics of the amyloid β-protein (Aβ) has direct relevance to the development of therapeutic agents for Alzheimer disease. To elucidate these dynamics, we combined scanning amino acid substitution with a method for quantitative determination of the Aβ oligomer frequency distribution, photo-induced cross-linking of unmodified proteins (PICUP), to perform "scanning PICUP." Tyr, a reactive group in PICUP, was substituted at position 1, 10, 20, 30, or 40 (for Aβ40) or 42 (for Aβ42). The effects of these substitutions were probed using circular dichroism spectroscopy, thioflavin T binding, electron microscopy, PICUP, and mass spectrometry. All peptides displayed a random coil → α/β → β transition, but substitution-dependent alterations in assembly kinetics and conformer complexity were observed. Tyr[1]-substituted homologues of Aβ40 and Aβ42 assembled the slowest and yielded unusual patterns of oligomer bands in gel electrophoresis experiments, suggesting oligomer compaction had occurred. Consistent with this suggestion was the observation of relatively narrow [Tyr[1]]Aβ40 fibrils. Substitution of Aβ40 at the C terminus decreased the population conformational complexity and substantially extended the highest order of oligomers observed. This latter effect was observed in both Aβ40 and Aβ42 as the Tyr substitution position number increased. The ability of a single substitution (Tyr[1]) to alter Aβ assembly kinetics and the oligomer frequency distribution suggests that the N terminus is not a benign peptide segment, but rather that Aβ conformational dynamics and assembly are affected significantly by the competition between the N and C termini to form a stable complex with the central hydrophobic cluster.**

Alzheimer disease (AD)[4] is the most common cause of late-life dementia (1) and is estimated to afflict more than 27 million people worldwide (2). An important etiologic hypothesis is that amyloid β-protein (Aβ) oligomers are the proximate neurotoxins in AD. Substantial *in vivo* and *in vitro* evidence supports this hypothesis (3–12). Neurotoxicity studies have shown that Aβ assemblies are potent neurotoxins (5, 13–20), and the toxicity of some oligomers can be greater than that of the corresponding fibrils (21). Soluble Aβ oligomers inhibit hippocampal long term potentiation (4, 5, 13, 15, 17, 18, 22) and disrupt cognitive function (23). Compounds that bind and disrupt the formation of oligomers have been shown to block the neurotoxicity of Aβ (24, 25). Importantly, recent studies in higher vertebrates (dogs) have shown that substantial reduction in amyloid deposits in the absence of decreases in oligomer concentration has little effect on recovery of neurological function (26).

Recent studies of Aβ oligomers have sought to correlate oligomer size and biological activity. Oligomers in the supernatants of fibril preparations centrifuged at 100,000 × g caused sustained calcium influx in rat hippocampal neurons, leading to calpain activation and dynamin 1 degradation (27). Aβ-derived diffusible ligand-like Aβ42 oligomers induced inflammatory responses in cultured rat astrocytes (28). A 90-kDa Aβ42 oligomer (29) has been shown to activate ERK1/2 in rat hippocampal slices (30) and bind avidly to human cortical neurons (31), in both cases causing apoptotic cell death. A comparison of the time dependence of the toxic effects of the 90-kDa assembly with that of Aβ-derived diffusible ligands revealed a 5-fold difference, Aβ-derived diffusible ligands requiring more time for equivalent effects (31). A 56-kDa oligomer, "Aβ*56," was reported to cause memory impairment in middle-aged transgenic mice expressing human amyloid precursor protein (32). A nonamer also had adverse effects. Impaired long term potentiation in rat brain slices has been attributed to Aβ trimers identified in media from cultured cells expressing human amyloid precursor protein (33). Dimers and trimers from this medium also have been found to cause progressive loss of synapses in organotypic rat hippocampal slices (10). In mice deficient in neprilysin, an enzyme that has been shown to degrade Aβ *in vivo* (34), impairment in neuronal plasticity and cognitive function correlated with significant increases in Aβ dimer levels and synapse-associated Aβ oligomers (35).

The potent pathologic effects of Aβ oligomers provide a compelling reason for elucidating the mechanism(s) of their

random coil; RP-HPLC, reversed phase-high performance liquid chromatography; ThT, thioflavin T; Tricine, N-[2-hydroxy-1,1-bis(hydroxymethyl)ethyl]glycine; SEC, size exclusion chromatography.

```
Aβ40                DAEFRHDSGYEVHHQKLVFFAEDVGSNKGAIIGLMVGGVV
[Phe¹⁰]Aβ40         ---------F------------------------------
[Tyr¹ ]Aβ40         Y--------F------------------------------
[Tyr²⁰]Aβ40         ---------F---------Y--------------------
[Tyr³⁰]Aβ40         ---------F-------------------Y----------
[Tyr⁴⁰]Aβ40         ---------F------------------------------Y

Aβ42                DAEFRHDSGYEVHHQKLVFFAEDVGSNKGAIIGLMVGGVVIA
[Phe¹⁰]Aβ42         ---------F-------------------------------
[Tyr¹ ]Aβ42         Y--------F-------------------------------
[Tyr²⁰]Aβ42         ---------F---------Y---------------------
[Tyr³⁰]Aβ42         ---------F-------------------Y-----------
[Tyr⁴²]Aβ42         ---------F-------------------------------Y
```

FIGURE 1. **Primary structure of Aβ peptides.** The sequences of wild type Aβ40 and Aβ42 are presented, *below* which are the sequences of the substituted peptides. *Hyphens* indicate identical amino acid residues. In peptides in which the Tyr probe was placed at positions other than the native position 10, a Phe group was substituted at position 10. For simplicity, these Aβ homologues are specified only by the position of the Tyr, *i.e.* [Tyr$^n$]Aβ40/42. The complete peptide specification would include the positions of both the Tyr and Phe residues, *e.g.* [Tyr$^n$,Phe$^{10}$]Aβ40/42.

formation. This has been a difficult task because of the metastability and polydispersity of Aβ assemblies (36). To obviate these problems, we introduced the use of the method of photoinduced cross-linking of unmodified proteins (PICUP) to rapidly (<1 s) and covalently stabilize oligomer mixtures (for reviews see Refs. 37, 38). Oligomers thus stabilized no longer exist in equilibrium with monomers or each other, allowing determination of oligomer frequency distributions by simple techniques such as SDS-PAGE (37). Recently, to obtain population-average information on contributions to fibril formation of amino acid residues at specific sites in Aβ, we employed a scanning intrinsic fluorescence approach (39). Tyr was used because it is a relatively small fluorophore, exists natively in Aβ, and possesses the side chain most reactive in the PICUP chemistry (40). Using this approach, we found that the central hydrophobic cluster region (Leu$^{17}$–Ala$^{21}$) was particularly important in controlling fibril formation of Aβ40, whereas the C terminus was the predominant structural element controlling Aβ42 assembly (39). Here we present results of studies in which key strategic features of the two methods have been combined to enable execution of "scanning PICUP" and the consequent revelation of site-specific effects on Aβ oligomerization.

## EXPERIMENTAL PROCEDURES

*Chemicals and Reagents*—Chemicals were obtained from Sigma and were of the highest purity available. Water was double-distilled and deionized using a Milli-Q system (Millipore Corp., Bedford, MA).

*Peptide Design and Synthesis*—In addition to studying native Aβ40 and Aβ42, each of which contains Tyr$^{10}$, single Tyr substitutions were made in each Aβ alloform at Asp$^1$, Phe$^{20}$, Ala$^{30}$, and the C terminus (Val$^{40}$ or Ala$^{42}$) (Fig. 1). In each non-native peptide, Tyr$^{10}$ was replaced by Phe, which is largely unreactive in PICUP, so that data interpretation would not be complicated by multiple potential cross-linking sites. A similar substitution strategy proved effective in Tyr intrinsic fluorescence studies

(39) in which Phe was fluorometrically, as opposed to chemically, insignificant. Aβ synthesis, purification, and characterization were done as described (41). Briefly, Aβ40, Aβ42, and their Tyr-substituted peptides (Fig. 1) were made on an automated peptide synthesizer (model 433A, Applied Biosystems, Foster City, CA) using Fmoc (*N*-(9-fluorenyl)methoxycarbonyl)-based methods. Peptides were purified using reversed phase high performance liquid chromatography (RP-HPLC). Quantitative amino acid analysis and mass spectrometry yielded the expected compositions and molecular weights, respectively, for each peptide. Purified peptides were stored as lyophilizates at −20 °C. When possible, to maximize chemical homogeneity among related peptides, multiple peptides were synthesized from the same starting resin by resin splitting at sites of sequence variation. Aβ40 and its Tyr-substituted analogues were synthesized using preloaded [Val]Wang resin. Aβ42 and its Tyr-substituted analogues were made in an analogous manner using preloaded [Ala]Wang resin. Peptides [Tyr$^{40}$]Aβ40 and [Tyr$^{42}$]Aβ42 were synthesized using preloaded [Tyr]Wang resin.

*Sample Preparation*—All peptides were pretreated with dilute NaOH to increase their solubility and decrease *de novo* peptide aggregation (42). Briefly, peptides were dissolved initially in 2 mM NaOH (1 mg/ml), sonicated for 3 min in an ultrasonic water bath (model B1200-R, Branson Ultrasonics Corp., Danbury, CT), and then lyophilized. This treatment and other treatments designed to produce unaggregated "starting" peptide preparations have not been found to affect the primary structure of the peptide or its subsequent folding and self-assembly (21, 42–46).

For CD studies, lyophilizates of pretreated peptides were dissolved in 1 volume of water, after which an equal volume of 20 mM phosphate buffer, pH 7.4, containing 0.02% (w/v) sodium azide was added. Samples were sonicated for 1 min at 22 °C, transferred into centrifugal filters (10,000 molecular weight cutoff, Centricon YM-10, Millipore Corp.), and centrifuged at 16,000 × *g* using a bench top microcentrifuge (Eppendorf model 5415C, Brinkmann Instruments) for 30 min. The filtrate, containing low molecular weight (LMW) Aβ, was incubated at 22 °C without agitation to allow peptide assembly. By definition (47), LMW Aβ contains monomeric Aβ in equilibrium with low order, unstructured oligomers (47–49). The concentration of Aβ in the filtrates was determined by quantitative amino acid analysis, as described (50).

For cross-linking experiments of Aβ40, LMW Aβ was isolated using size exclusion chromatography (SEC), as described (41). Briefly, Aβ was dissolved at a concentration of 2 mg/ml in dimethyl sulfoxide and sonicated for 1 min, after which 170 μl of this solution was injected onto the SEC column. The column

was eluted with 10 mM sodium phosphate buffer, pH 7.4, at a flow rate of 0.5 ml/min. Peptides were detected by UV absorbance at 254 nm, and fractions of 350-μl volume were collected during elution of the LMW Aβ peak. The concentrations of Tyr-substituted Aβ42 peptides isolated by SEC were lower than those obtained using the centrifugation method (51); therefore, the latter method was used to prepare Aβ42 peptides for study. Both peptide preparation methods yielded Aβ solutions that produced CD spectra indicative of predominantly disordered secondary structure. Previous studies have shown that LMW Aβ42 prepared using filtration or SEC produces similar oligomer distributions in the monomer to octamer region (48). An advantage of the filtration method for preparing Aβ42 is that larger oligomers (*e.g.* dodecamers and octadecamers) are not present (48).

*Cross-linking and SDS-PAGE Analysis*—Peptides were covalently cross-linked using PICUP immediately after preparation (for a review see Ref. 38). Briefly, 1 μl of 1 mM Tris(2,2′-bipyridyl)dichlororuthenium(II) and 1 μl of 20 mM ammonium persulfate in 10 mM sodium phosphate, pH 7.4, were added to 18 μl of a 20–30 μM solution of Aβ or its analogues immediately after preparation. The mixture was irradiated for 1 s with visible light, and the reaction was quenched immediately with 10 μl of Tricine sample buffer (Invitrogen) containing 5% (v/v) β-mercaptoethanol. The cross-linked oligomer mixtures were fractionated by SDS-PAGE using 10–20% Tricine gels (1.0 mm × 10 well) (Invitrogen) and silver-stained using a SilverXpress silver staining kit (Invitrogen), and then the band intensities were quantified by densitometry, as described (49). The amounts taken for SDS-PAGE analyses were adjusted according to the peptide concentration, determined by amino acid analysis, so that equal amounts of protein were loaded in each lane. Gels were dried and scanned, and the intensities and gel mobilities ($R_f$) of the resulting monomer and oligomers bands were quantified by densitometry using the program One-Dscan (Scanalytics, Fairfax, VA). The relative amount of each band in a lane as a percentage of all bands in the same lane ($I_r^i$) was determined according to Equation 1,

$$I_r^i = (I_i / \Sigma I_i) \times 100 \qquad \text{(Eq. 1)}$$

where $I_i$ is the intensity of the band *i*.

*Circular Dichroism Spectroscopy*—Aβ, at a concentration of 30–35 μM in 10 mM phosphate buffer, pH 7.4, was prepared by filtration, and the spectra were acquired daily during incubation of peptides at 22 °C without agitation. Samples were prepared for analysis by gently drawing up and then expelling the peptide solution in a 200-μl pipette tip. After three such cycles, the peptide solution was placed into a 0.1-cm path length quartz cell (Hellma, Forest Hills, NY). Spectra were acquired using an Aviv model 62A DS spectropolarimeter (Aviv Associates, Lakewood, NJ). Following measurements, samples were returned to the original sample tubes. All measurements were done at 22 °C. Spectra were generally recorded over the wavelength range of 198–260 nm. Three independent experiments were performed with each peptide. Raw data were manipulated by smoothing and subtraction of buffer spectra, according to the manufacturer's instructions.

Spectral deconvolution was performed using the CDPro software package (52), which contains the deconvolution programs SELCON3, CDSSTR, and CONTIN. In this package, reference sets of proteins from different sources are combined to create a large reference set of CD spectra. Depending on the spectrum wavelength range, the number of proteins in the reference set (IBasis) can be as large as 48 (IBasis 7). Deconvolutions were done with each of the three programs. If the data thus obtained were similar, they were averaged to obtain the percentage of each secondary structure element. In some cases, the results obtained from one program were highly divergent from those of the other two. In this case, averaging was done only with data from the two consistent programs. Deconvolutions were performed on data acquired at the initiation of assembly, when the presence of significant α-helix was observed (by visual inspection of the spectra), and when assembly was complete (spectra remained identical during repeated monitoring). We note that the kinetics of assembly in these studies differ quantitatively, but not qualitatively, from those acquired in previous work (53). Here, the assembly reactions were performed using 20 mM phosphate buffer, pH 7.4. The earlier studies were done in 10 mM Gly-NaOH, pH 7.5. The latter buffer slows the kinetics and facilitates occupation of regions of conformational space containing α-helix.

*Thioflavin T (ThT) Binding*—A 100-μl aliquot of each Aβ sample in 10 mM phosphate buffer, pH 7.4, containing 0.01% (w/v) sodium azide, was mixed with 5 μl of 100 μM ThT prepared in the same buffer. Immediately after addition of ThT, fluorescence was measured. The measurements were made using a Hitachi F4500 spectrofluorometer (Hitachi Instruments Inc., Rye, NH) with excitation at 450 nm and emission at 480 nm. A rectangular 10-mm quartz microcuvette was used. All fluorescence measurements were carried out at 22 °C with a scan rate of 240 nm/min. Slit widths used for excitation and emission were 5 and 10 nm, respectively. Three independent experiments were performed for each peptide.

*Electron Microscopy*—For studies of fibrillar Aβ, 5 μl of each sample were spotted on a glow-discharged, carbon-coated Formvar grid (Electron Microscopy Sciences, Fort Washington, PA), incubated for 5 min, washed with distilled water, and then stained with 1% (w/v) aqueous uranyl formate. Uranyl formate (Pfaltz & Bauer, Waterbury, CT) solutions were filtered through 0.2-μm sterile syringe filters (Corning Glass) before use. EM analysis was performed using a JEOL 1200 transmission electron microscope. Four independent experiments were carried out for each peptide.

For studies of cross-linked and noncross-linked LMW Aβ peptides, cross-linking reactions were quenched with 1 M dithiothreitol (FisherBiotech, Fair Lawn, NJ) in water instead of 5% (v/v) β-mercaptoethanol in Tricine sample buffer (Invitrogen). The same LMW preparation also was cross-linked and quenched immediately with 10 μl of 5% (v/v) β-mercaptoethanol in Tricine sample buffer and then used for SDS-PAGE to verify that the expected oligomer distribution was obtained. Ten μl of each sample were incubated for ~20 min on the grid. The solution was gently removed using Whatman grade 2 qualitative filter paper, and then the grid was incubated with 5 μl of 2.5% (v/v) glutaraldehyde for 4 min, after which fluid again was

removed using filter paper. The peptide then was stained with 5 μl of 1% (w/v) uranyl acetate (Pfaltz & Bauer) for 3 min. This solution was wicked off, and the grid was air-dried. Samples were examined using a JEOL CX100 electron microscope.

Quantitative analysis of oligomer geometry in cross-linked and noncross-linked LMW Aβ samples was performed by manual determination of oligomer dimensions by inspection of EM images. A representative sample was obtained with particle number $n = 40$. Particle diameter and length statistics were calculated using Mathematica 6.0 (Wolfram Research, Inc., Champaign, IL).

*Reverse Staining and Isolation of Individual Oligomers*— Cross-linked Aβ oligomers separated by SDS-PAGE were detected by imidazole-zinc staining, essentially as described (54). Briefly, after SDS-PAGE, the gel was rinsed in distilled water for 30 s and then incubated in 0.2 M imidazole (Sigma) solution containing 0.1% (w/v) electrophoresis grade SDS (Fisher) for 15 min. The solution then was discarded, and the gel was incubated in 0.2 M zinc sulfate in distilled water for ~0.5–1 min, until the gel background became white and the Aβ oligomers bands were transparent and colorless. Further staining was prevented by rinsing the gel in distilled water. The staining process was monitored by placing the gel in a transparent tray over a piece of black paper. Immediately after staining, the oligomer bands were excised using a scalpel blade (Fisher) and placed into 1.5-ml conical microcentrifuge tubes. The gel slices were incubated (two times for 5 min each) in 1 ml of 25 mM ammonium acetate buffer, pH 7.4, containing 100 mM EDTA, during which time the gels become completely colorless. The gel slices then were washed twice (two times for 5 min each) using 25 mM ammonium acetate buffer, pH 7.4, and frozen quickly on dry ice (to make the gels pieces brittle and fragile). The pieces were crushed using a 1.5-ml microcentrifuge tube as a mortar and a geometrically matched pestle (Fisher). After crushing the gel pieces, the pestle was held over the tube and washed with 25 mM ammonium acetate buffer, pH 7.4, to ensure that all the gel pieces were collected. Additional buffer was added to the tube to make the volume of the resulting suspension twice that of the original gel pieces. The microcentrifuge tube containing the gel suspension then was agitated by moderate vortexing for 10 min using a Multi-Tube Vortexer (VWR International, Bristol, CT). The gel mixture was centrifuged for ~1 min at 14,000 × g, and the supernatant was then collected and placed in a glass tube. A volume of buffer twice that of the crushed gel was added to the pellet, which then was vortexed for 10 min. After another centrifugation, done as above, the supernatant was collected and combined with the first supernatant. A volume of 25 mM ammonium acetate, 50% (v/v) acetonitrile, 0.1% (v/v) trifluoroacetic acid, equal to that of the pellet, was then added to the pellet, and the tube was vortexed for 10 min. A third supernatant then was obtained by centrifugation and was combined with the first two supernatants. Because Aβ oligomers are hydrophobic, a fourth extraction was done for 10 min using 25 mM ammonium acetate buffer, 25% (v/v) acetonitrile, 25% (v/v) isopropyl alcohol, and 0.1% (v/v) trifluoroacetic acid. A final extraction was done for 2 min using 80% (v/v) acetonitrile. The pooled supernatants were concentrated by centrifugal evaporation (Savant SpeedVac Concentrator, Thermo Scientific, Waltham, MA).

*Matrix-assisted Laser Desorption/Ionization-Mass Spectrometry (MALDI-MS)*—MALDI-MS was performed on a Voyager-DESTR time-of-flight mass spectrometer (Applied Biosystems) employing 337 nm irradiation. The matrices α-cyano-4-hydroxycinnamic acid, sinapinic acid, ferulic acid, 2-mercaptobenzothiazole, norharmane, 2-(4-hydroxyphenylazo)benzoic acid, and 2,5-dihydroxybenzoic acid were investigated. The 2,5-dihydroxybenzoic acid matrix yielded superior spectra and thus was employed for all experiments described here. Mass spectra were acquired in linear and reflector modes. Oligomers were detected most readily in linear mode.

## RESULTS

*Secondary Structure Dynamics*—To probe amino acid site-specific contributions to peptide conformation and assembly, we used CD spectroscopy and ThT binding to monitor temporal changes in secondary structure. In the CD analyses, Aβ40 and its substituted alloforms were predominantly unstructured immediately after preparation, as indicated by prominent negative molar ellipticities at ~198 nm (Fig. 2A). Conformational changes in Aβ40 were noticeable after ~6 days. At day 7, mixed α/β character was indicated qualitatively by double inflections in the 205–225 nm region and quantitatively by spectral deconvolution. Visual inspection suggested that α-helix content was maximal at ~8 days. Quantitative analysis of the spectra was done following deconvolution (see "Experimental Procedures"). At 0 day, α-helix, β-strand, β-turn, and random coil (RC)[5] secondary structure elements were present at levels of ~8, ~9, ~6, and 77%, respectively. In contrast, at 8 days, α-helix, β-strand, β-turn, and RC levels were ~26, ~24, ~19, and 33%, respectively. The mixed α/β conformer population at 8 days includes in part a previously described α-helix-rich intermediate (53). Between days 7 and 14, an α/β → β transition was observed that produced a classical β-sheet-type spectrum with a negative ellipticity of significant magnitude centered at ~215–218 nm. The spectral deconvolution at day 14 showed that the α-helix, β-strand, β-turn, and RC levels were ~10, ~66, ~5, and 20%, respectively.

[Phe[10]]Aβ40, the "scaffold" upon which the Tyr-substituted peptides was built, displayed time-dependent conformational changes qualitatively similar to that of Aβ40, as did the four other Tyr-substituted alloforms. As reported previously in studies of Aβ40 assembly (53), absolute convergence of the spectra onto an isodichroic point was not seen, suggesting a multistate transition process. We do note, however, that some convergence of the spectra to a single point occurred in the [Tyr[40]]Aβ40 experiment.

To obtain quantitative insight into the kinetics of the RC → α/β → β conformational conversions, we studied the time dependence of $\theta_{222}$ (supplemental Fig. 1A). The half-time for the development of α-helix structure and the time at which

---

[5] We use the term "random coil" to refer to an irregular conformational state characterized by a relative lack of well defined structural elements such as α-helices, β-sheets, or β-turns. We do not suggest that this state is truly random in nature.
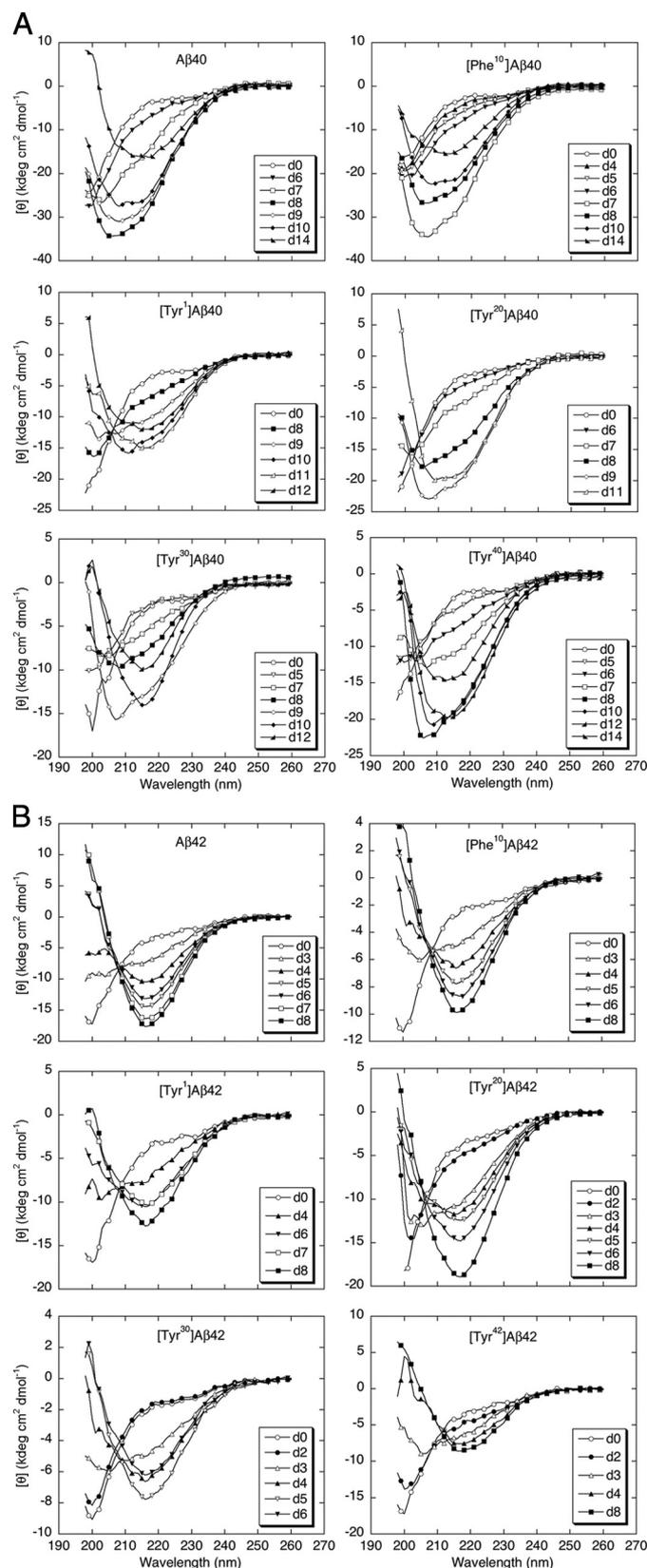
## A



## B



FIGURE 2. **Secondary structure dynamics.** *A,* Aβ40 and homologues were incubated in 10 mM phosphate buffer, pH 7.4, at 22 °C. CD spectra were acquired daily for 14 days. The day on which a spectrum was acquired is indicated by "*d.*" The spectra shown are the average of six scans each with an averaging time of 5 s. *B,* Aβ42 and homologues were analyzed in the same manner. Results for both sets of peptides are representative of those obtained in each of four independent experiments.

**TABLE 1**

**ThT binding**

Peptide samples were incubated at 22 °C at a concentration of ~30 $\mu$M in 10 mM phosphate, pH 7.4. ThT fluorescence intensity ($I$) was determined, as described under "Experimental Procedures," immediately after peptide preparation ($I_0$) or after assembly was complete ($I_t$ = 14 days for Aβ40 or 8 days for Aβ42), as judged by CD. $I$ is in fluorescence units ± S.D., where the units are arbitrary.

| Peptide | $I_0$ | $I_t$ |
|---|---|---|
| [Phe[10]]Aβ40 | 40 ± 11 | 9897 ± 698 |
| [Tyr[1]]Aβ40 | 36 ± 12 | 10,199 ± 501 |
| Aβ40 | 18 ± 6 | 9014 ± 416 |
| [Tyr[20]]Aβ40 | 21 ± 8 | 9936 ± 406 |
| [Tyr[30]]Aβ40 | 32 ± 9 | 8890 ± 355 |
| [Tyr[40]]Aβ40 | 42 ± 16 | 8912 ± 358 |
| [Phe[10]]Aβ42 | 37 ± 8 | 5607 ± 644 |
| [Tyr[1]]Aβ42 | 46 ± 10 | 4651 ± 696 |
| Aβ42 | 42 ± 12 | 5609 ± 502 |
| [Tyr[20]]Aβ42 | 43 ± 5 | 4950 ± 749 |
| [Tyr[30]]Aβ42 | 39 ± 7 | 2250 ± 825 |
| [Tyr[42]]Aβ42 | 51 ± 14 | 4780 ± 612 |

maximal $\alpha$-helix structure is observed are later for [Tyr[1]]Aβ40 (8.5 and 11 days, respectively) than they are for Aβ40 (7 and 8 days, respectively). These two times also are longer than those for [Tyr[10]]Aβ40 or [Tyr[20]]Aβ40. The half-time for [Tyr[30]]Aβ40 (8 days) is slightly earlier than that of [Tyr[1]]Aβ40, but the $\alpha$-helix maximum occurs at least 2 days earlier. [Tyr[40]]Aβ40 displays a significantly earlier half-time (7 days) and a slow conformational transition that extends for at least 4 days. Smoothing of these data would suggest that the $\alpha$-helix maximum for [Tyr[40]]Aβ40 occurs at least 1 day earlier than that in [Tyr[1]]Aβ40.

Consistent with the CD studies, no ThT binding was observed by any peptides immediately after their preparation (Table 1). However, substantial binding was detected when characteristic $\beta$-sheet spectra were seen by CD. Binding levels among the different peptides were equivalent, within experimental error (FU$_{avg}$ = 9475 ± 598), where FU is fluorescence units.

CD analysis revealed that Aβ42, [Phe[10]]Aβ42, and the Tyr-substituted analogues displayed RC $\rightarrow \alpha/\beta \rightarrow \beta$ transitions (Fig. 2*B*) qualitatively similar to those observed with Aβ40, but with accelerated kinetics. Consistent with this acceleration, the observed lifetimes of the $\alpha$-helix-containing conformers were relatively short (1 day instead of 3–5 days in Aβ40). The $\alpha$-rich conformer appeared for all peptides at day 3, except for [Tyr[1]]Aβ42, in which the $\alpha$-helix-rich conformer appeared at day 4. The rapidity with which the RC $\rightarrow \alpha/\beta \rightarrow \beta$ transition occurs in the Aβ42 peptide family is indicated by a monotonic decrease in $\theta_{222}$ that begins earlier and does not reach the magnitude of those seen in the Aβ40 samples (supplemental Fig. 1*B*). This increased Aβ42 assembly rate is consistent with results of earlier comparative studies of Aβ40 and Aβ42 peptides linked to familial forms of AD and cerebral amyloid angiopathy (53).

Deconvolution of the Aβ42 spectra obtained immediately following preparation of LMW peptides revealed levels of $\alpha$-helix, $\beta$-strand, $\beta$-turn, and RC of ~4–5, ~12–15, ~10–15, and ~65–70%, respectively. At the midpoints of the RC $\rightarrow \alpha/\beta \rightarrow \beta$ conformational transitions, levels of $\alpha$-helix, $\beta$-strand, $\beta$-turn, and RC were ~12–16, ~35, ~20, and ~30%, respectively.

The spectral deconvolution at day 8, where all Aβ42 spectra were mostly $\beta$-sheet (by visual inspection), confirmed that all
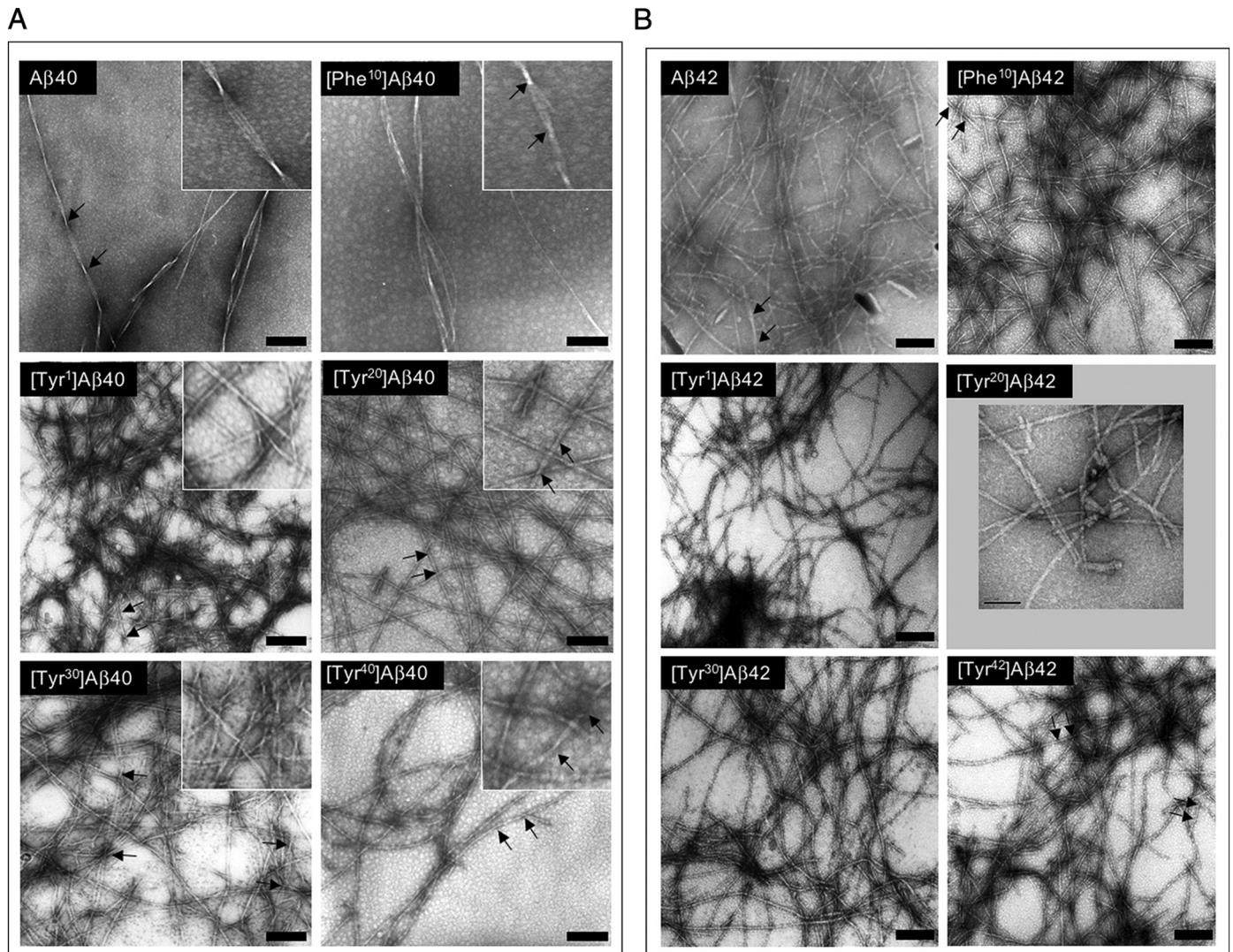
**A**



**B**

FIGURE 3. **Morphology of Aβ assemblies.** Following peptide assembly, transmission electron microscopy was performed on negatively stained samples as follows: *A,* Aβ40 and homologues; *B,* Aβ42 and homologues. The numerous small (<5 nm), translucent background structures visible to various degrees in the panels are not proteinaceous but rather are artifacts of the staining procedure. Protein structures of these sizes are not observed in experiments in which fibril formation is allowed to proceed to completion. *Scale bars,* 100 nm. *Insets* in *A* are higher magnification images of the respective fields. The *insets* are 133 nm square. *Arrows* delimit helical pitches discussed in the text.

Aβ42 peptides had abundant β-sheet (~70%)-rich structure. The α-helix and RC content were ~5 and ~20%, respectively. In contrast to the Aβ40 series, an isodichroic point was observed at a wavelength of ~210 nm in experiments on the Aβ42 peptide series. This point was particularly prominent in Aβ42 and [Phe[10]]Aβ42 but also was present in the four other samples. Interestingly, the most divergent spectrum in each of these four samples was obtained at the time of maximal α-helix content, and among these, the [Tyr[30]]Aβ42 was the most divergent. No ThT binding was observed initially, but significant binding was detected when β-sheet-like CD spectra existed (Table 1). With the exception of [Tyr[30]]Aβ42, all the Aβ42 peptides bound equivalent amounts of ThT ($FU_{avg}$ = 4641 ± 1241). [Tyr[30]]Aβ42 produced ~½ the ThT fluorescence as did the average Aβ42 peptide, and the Aβ42 average ThT binding was ~½ that of the average Aβ40 peptide.

It should be noted that the reproducibility of studies of Aβ assembly kinetics depends on careful peptide preparation and manipulation (for a recent review see Ref. 36). The experiments presented here all were performed using the same peptide lot that was prepared and incubated in precisely the same manner for all samples. Solutions were not agitated and any study of the reactions was done with minimal perturbation of the tubes. Under these conditions, the kinetics was reproducible within experiments. Absolute changes in kinetics can be observed between experiments, but the rank order of rates of conformational change remains constant among experiments. Thus, peptides that form the β-sheet structure the fastest in any one experiment always form the β-sheet structure the fastest. Similarly, the "slowest" peptides always are the slowest. The system variability thus is so small that the trends in rank order of β-sheet formation are always the same.

*Morphologic Analysis of Assemblies*—To determine the morphologies of the assemblies present at the completion of the CD and ThT studies, EM was done. All 12 peptides formed long, unbranched fibrils with smooth margins (Fig. 3, *A* and *B*). Aβ40
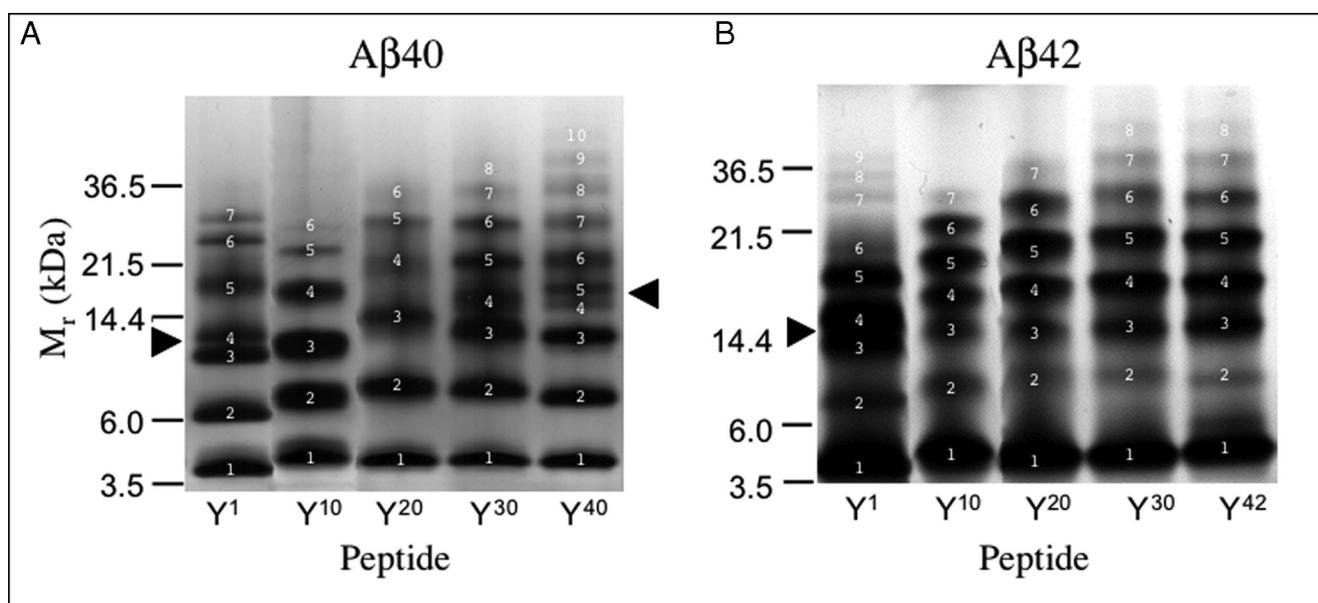
FIGURE 4. **Oligomer size distributions.** *A,* Aβ40 and homologues were cross-linked using PICUP, and then oligomer frequency distributions were determined by SDS-PAGE followed by silver staining. Molecular masses of protein standards are shown on the *left*. The gels are representative of each of three independent experiments. *B,* Aβ42 and homologues analyzed as in *A.* The *arrowheads* indicate regions in which band migration differed from that of the corresponding wild type peptide (see text). *White numbers* specify band numbers.

produced 8 – 12 nm diameter fibrils comprising three individual filaments of ~3.3 nm diameter twisted into a helical superstructure with a pitch 150 – 160 nm. [Phe[10]]Aβ40, [Tyr[20]]Aβ40, and [Tyr[40]]Aβ40 fibrils typically were composed of two laterally associated filaments wound together with a helical pitch of ~75 – 110 nm. [Tyr[1]]Aβ40 and [Tyr[30]]Aβ40 produced a more structurally diverse population of fibrils that displayed diameters ranging from 6 to 12 nm and were composed of 2–5 filaments. Some fibrils had no observable twist, whereas others displayed a helical pitch of ~100 – 150 nm.

In contrast to the variation in fibril morphologies observed in the Aβ40 samples (Fig. 3*A*), Aβ42 peptides formed fibrils that were morphologically similar (Fig. 3*B*). Most fibrils were ~4 – 6 nm in diameter and were composed of two filaments. Little discernible substructure was apparent in many fibrils, whereas others appeared with irregular twists or helical twists with pitches of ~40 – 80 nm. The only departure from these shared morphologic features was observed with [Phe[10]]Aβ42, which produced fibrils with a diameter range, 5–7.5 nm, that overlapped with but was slightly larger than that of the other peptides. The largest fibril included three filaments. The approximate 2-fold difference in diameter between fibrils formed by Aβ40 and Aβ42 is consistent with and provides a plausible explanation for the magnitude of the difference in ThT binding observed between the two peptide families (see above). However, this explanation assumes a linear relationship between ThT binding and fluorescence intensity. It also is possible that variations in average order or self-quenching could account for the observed differences.

*Determination of Oligomer Size Distributions*—To probe Aβ oligomerization, LMW fractions of Aβ and its Tyr-substituted alloforms were isolated and immediately analyzed by PICUP and SDS-PAGE (Fig. 4 and supplemental Table 1). Distinct oligomer size distributions were observed. Aβ40 ([Tyr[10]]Aβ40)

produced a mixture consisting of predominantly monomer (~20%), dimer (~25%), trimer (~25%), and tetramer (~17%), along with small amounts of pentamer (~6%) and hexamer (~3%). The oligomer distribution of [Tyr[1]]Aβ40 differed from that of Aβ40. Presumptive [Tyr[1]]Aβ40 monomers through trimers electrophoresed slightly faster than wild type monomer, dimers, and trimers. In the gel region corresponding to the native trimer, two bands existed (Fig. 4, *closed arrowhead*). Above this region, three additional prominent bands were seen. The oligomer distributions of [Tyr[20]]Aβ40, [Tyr[30]]Aβ40, and [Tyr[40]]Aβ40 also differed from that of the wild type. A large shift to a higher $M_r$ was observed for the presumptive trimer band and higher order oligomers of [Tyr[20]]Aβ40. The distribution of [Tyr[30]]Aβ40 resembled that of [Tyr[1]]Aβ40 in that bands 3 and 4 migrated close to each other, like a doublet. In addition, the $M_r$ values for the higher order oligomers were higher than those of the corresponding Aβ40 oligomers, and at least one or two higher order oligomer bands were observed (band 7 and above). Cross-linking of [Tyr[40]]Aβ40 produced the greatest number of bands (10 bands). The [Tyr[40]]Aβ40 distribution was similar to that of Aβ40 in the monomer-trimer region, but a doublet was formed by bands 4 and 5 (see Fig. 4, *arrowhead*).

All the substitutions caused increases in the number of oligomer bands and the $M_r$ of the highest order band. These effects were most apparent in the peptides in which substitutions were made at the C terminus (positions 30 and 40/42). We note also that the migration differences of dimers and trimers in the substituted peptides relative to Aβ40 were greatest in [Tyr[20]]Aβ40 and progressively smaller in [Tyr[30]]Aβ40 and [Tyr[40]]Aβ40.

Cross-linking of Aβ42 produced a characteristic (48) distribution with nodes at monomer and pentamer. Heptamers were visible clearly. In the [Tyr[1]]Aβ42 distribution, the predominant oligomer was the tetramer (Fig. 4, *closed arrowhead*). Interest-
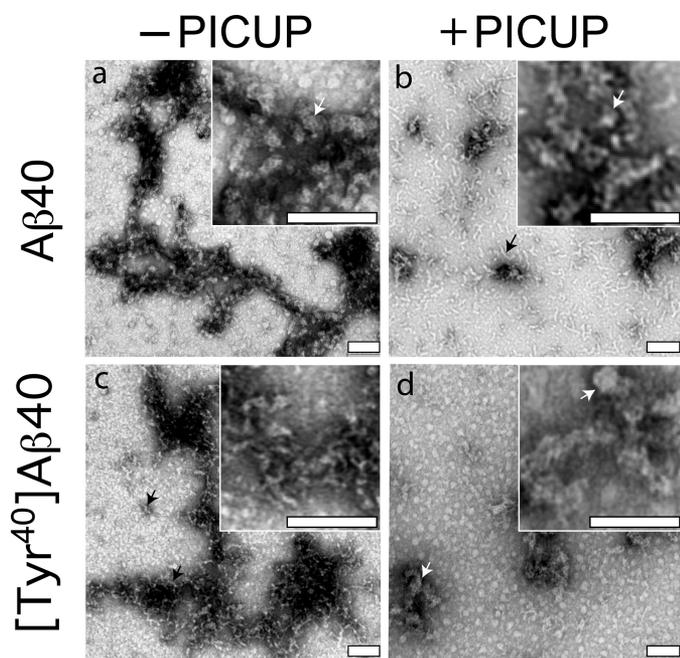
FIGURE 5. **Morphologic analysis of cross-linked peptides.** The morphologies of uncross-linked (−PICUP) (*a* and *c*) and cross-linked (+PICUP) (*b* and *d*) wild type and Tyr[1]-substituted Aβ40 peptides, respectively, were determined by EM of negatively stained preparations. *Scale bars,* 100 nm. The images are representative of those in each of at least three independent experiments. *Arrows* identify structures discussed in the text.

ingly, the oligomer distribution in the [Tyr[1]]Aβ42 sample was similar to that of the [Tyr[1]]Aβ40 sample. The $M_r$ values of the bands were lower than those of wild type Aβ42 and bands 3 and 4 migrated as a doublet. In addition, a larger number of bands were seen (9 *versus* 7), and the largest $M_r$ exceeded heptamer. The oligomer distributions of the Tyr[20], Tyr[30], and Tyr[42] alloforms showed $M_r$ values of tetramers and higher order oligomers higher than their Aβ42 homologue. In addition, as with Aβ40, all the substitutions caused increases in the number of oligomer bands and the $M_r$ of the highest order band, and these effects were most apparent in the peptides in which substitutions were made at the C terminus (positions 30 and 42).

We note that, at the peptide concentrations used in these experiment, small variations in experimental conditions (peptide and reactant concentrations, temperature, irradiation time, etc.) do not alter significantly the oligomer frequency distributions. These distributions were reproducible among experiments. Importantly, based on careful study of the cross-linking system itself (49) and on results of extensive structure-activity studies (38, 48, 49), the differences observed among samples in the oligomer frequency distribution and $M_r$ values of individual bands are meaningful. The data are not due to random collisional events "captured" by cross-linking.

*Determination of Oligomer Morphology*—To determine whether increased oligomerization propensity, as indicated by expansion of the oligomer distribution range to higher molecular weight, was reflected in increased oligomer size, EM studies were performed. Among all the peptides studied, Aβ40 and [Tyr[40]]Aβ40 displayed the largest difference in oligomerization propensity, and thus we determined their morphologies immediately following isolation by SEC and cross-linking by PICUP (Fig. 5).

Both noncross-linked and cross-linked Aβ40 displayed clusters of relatively amorphous structures with low aspect ratios. The average diameter of the globular structures seen in noncross-linked Aβ40 was 16.0 ± 0.54 nm (Fig. 5*a, inset, white arrow*), and 93% of these globules had diameters between 12 and 20 nm (supplemental Fig. 2*A*). Aggregates often were observed. Cross-linked Aβ40 produced aggregates that were more thread-like in appearance (Fig. 5*b, black arrow*) but had similar average diameters (15.8 ± 0.61 nm; Fig. 5*b, inset, white arrow*, and supplemental Fig. 2*B*). Short protofibril-like structures were also observed, and these were more frequent in the cross-linked sample. The lengths of these structures varied significantly (~11–111 nm; supplemental Fig. 2*C*), but the distribution of average diameter ($\bar{d}$) was narrow ($\bar{d} = 6.2 ± 0.2$ nm; supplemental Fig. 2*D*).

Non cross-linked [Tyr[40]]Aβ40 also produced relatively amorphous globules and thread-like structures (Fig. 5*c, black arrows*). The average diameter of these particles was 9.7 ± 1 nm (supplemental Fig. 2*E*), smaller than that of Aβ40. However, the range of lengths of protofibril-like assemblies produced by [Tyr[40]]Aβ40 was similar to that of Aβ40 (15–100 nm; supplemental Fig. 2*F*). The average diameter of the amorphous structures formed in the cross-linked [Tyr[40]]Aβ40 sample (Fig. 5*d, white arrows*), 19.6 ± 0.9, was approximately twice that of the noncross-linked peptide and significantly ($p < 0.0001$) larger than that of cross-linked Aβ40 (supplemental Fig. 2*G*). This increase is consistent with the increased order observed in the SDS gels of the cross-linked peptides (Fig. 4).

We note, in principle, that a direct correspondence between PICUP and EM may not be observed because the former method uses the denaturing and dissociative characteristics of SDS-PAGE to reveal covalent association among monomers, whereas the latter method requires only adherence of aggregates to a solid support and not their *pre facto* covalent association. Here, however, the data produced by each method are consistent.

*Determination of Oligomer Order*—Our analyses of the oligomer size distributions of the Tyr-substituted peptides (Fig. 4) revealed that certain substitutions, *e.g.* [Tyr[1]]Aβ40, produced oligomer distributions distinct from those of wild type Aβ. To determine the oligomer order within the various gel bands, their component peptides were isolated and subjected to MALDI-TOF mass spectrometry. We first determined the mass of all oligomer bands from wild type Aβ40 (band numbers are shown in Fig. 4 with *white letters*). Band 1 from Aβ40 produced a major peak of 4332 atomic mass units with an additional small broad peak (<5%) of 8574 atomic mass units. We assigned the 4332 atomic mass unit peak to the singly protonated Aβ40 monomer (theoretical *m/z* = 4331; Fig. 6*A*). Bands 2, 3, and 4 produced major peaks of 8656, 13,010, and 17,383 atomic mass units, corresponding to dimer, trimer, and tetramer, respectively (Fig. 6*A*). Masses from the higher order bands 5 and 6 could not be obtained, likely because the high molecular weight oligomers were present in small quantities, or they may not have been desorbed from the MALDI matrices as readily as the smaller oligomers. Mass spectrometric analysis thus confirmed that Aβ40 produced a simple oligomer "ladder."
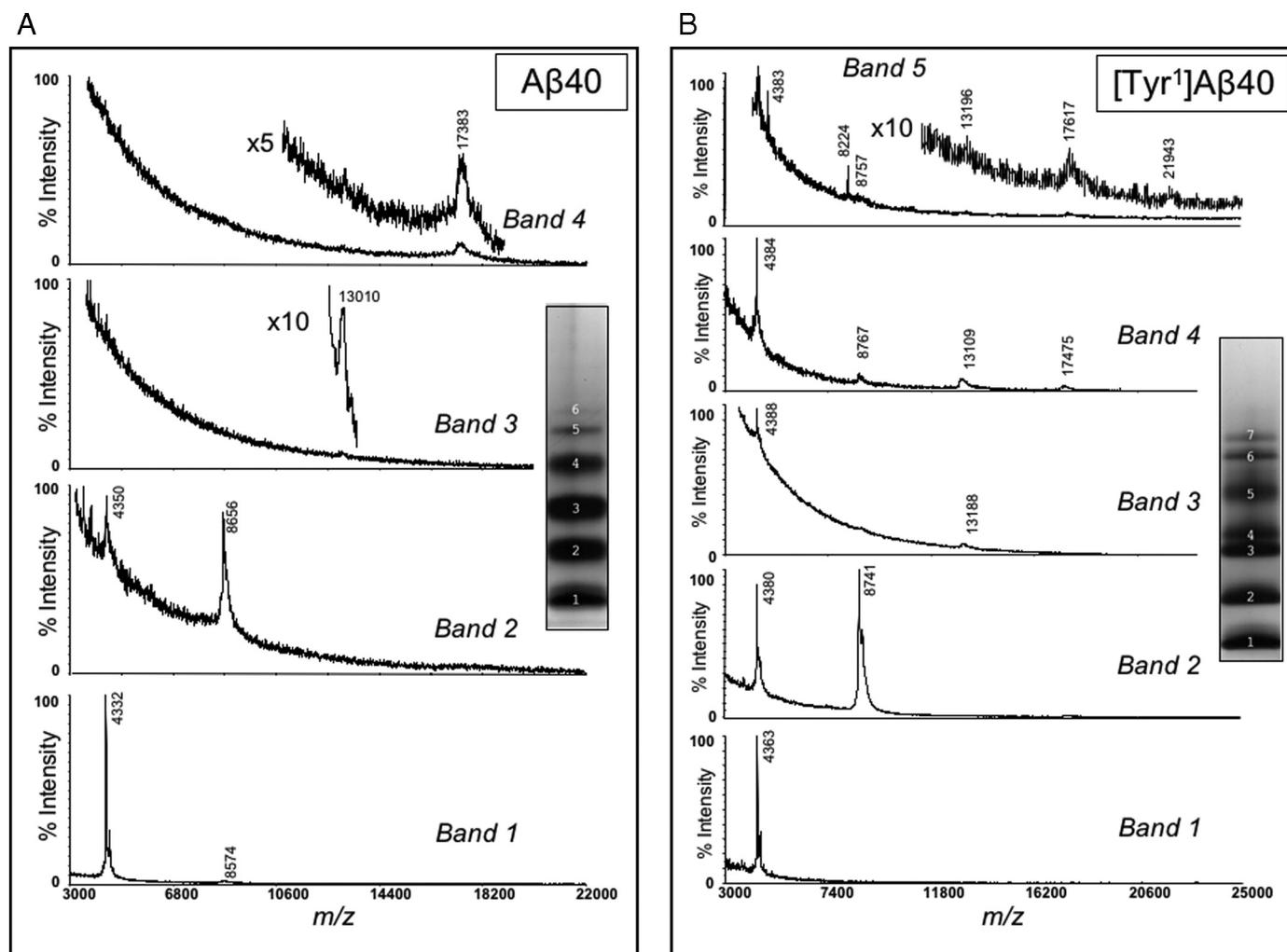
A



B

FIGURE 6. **MALDI-TOF MS analysis of isolated oligomers.** Bands produced by Aβ40 (*A*) and [Tyr[1]]Aβ40 (*B*) following PICUP and SDS-PAGE were identified by negative staining of the gels, after which the protein components were eluted and analyzed mass spectrometrically (see "Experimental Procedures"). Normalized ion intensities are presented on the *ordinates*, and mass-to-charge (*m/z*) ratios are presented on the *abscissas*. Band numbers and the locations of specific oligomers within the spectra are indicated. *Insets* show the actual gel lanes from which the bands were isolated.

We next analyzed [Tyr[1]]Aβ40 (Fig. 6*B*). Band 1 displayed a mass of 4363 atomic mass units, which is the average mass of a singly protonated monomer. In linear mode, band 2 produced two almost equally intense peaks, one at 8741 atomic mass units and one at 4380 atomic mass units. The ion of 4380 atomic mass units is consistent with oxidized [Tyr[1]]Aβ40 (expected mass of 4379 atomic mass units), whereas 8741 atomic mass units is consistent with a dimer in which one monomer is oxidized (expected mass of 8739 atomic mass units). A spectral component of mass 4363 atomic mass units also was observed, consistent with the presence of un-oxidized monomer. Measurements done in reflector mode revealed 1 atomic mass unit isotope spacings in the 4400 atomic mass units region, establishing that doubly charged ~8800-Da species were not solely responsible for the 4400 atomic mass units ions. Band 3 produced major ions of 4388 and 13,188 atomic mass units, consistent with monomer mass and trimer, respectively. Although the 13,188 atomic mass unit ion is ~100 Da higher in mass than expected for the trimer (13,090), it is reasonable to assign it to the trimer as other oligomers clearly could not produce such a mass. Band 4 yielded four significant peaks, the masses of which

were 4384, 8767, 13,109, and 17,475 atomic mass units. We assign these to peptide monomer, dimer, trimer, and tetramer, respectively. Band 5 displayed five peaks that were consistent in $M_r$ with oxidized monomer (4383), oxidized dimer (8757), oxidized trimer (13,196), oxidized tetramer (17,617), and oxidized pentamer (21,943). The data show, as with Aβ40, that an oligomer ladder was produced in the SDS-PAGE experiment that comprised neighboring oligomers differing in order by one. Importantly, the combined electrophoretic/spectroscopic analyses reveal that the Tyr[1] substitution significantly alters the $M_r$ of the peptide tetramer and pentamer, but it has much less effect on the monomer, dimer, and trimer. As with Aβ40 itself, sufficient signal could not be obtained to analyze the presumptive hexamer and heptamer bands of this peptide (Fig. 4, *bands 6* and *7*).

Despite extensive efforts using a broad range of matrices and solvents, spectra of [Tyr[1]]Aβ42 oligomers were not obtained. Insolubility did not appear to explain the phenomenon, as the dried analytes dissolved completely in the solvents employed. Rather, the result may be due to the follow-

ing: 1) the inability of these oligomers to be incorporated within crystals of the MALDI matrices, perhaps because of their exceptional hydrophobicity; or 2) the disruption of labile covalent bonds or weak noncovalent interactions by the desorption/ionization process.

## DISCUSSION

Evidence from *in vitro* and *in vivo* studies suggests that Aβ oligomers are potent neurotoxins and may be the proximal effectors of the neuronal dysfunction and death occurring in AD (4, 55–57). This strong association of Aβ oligomers with AD pathogenesis provides a rationale for the performance of studies to elucidate the structural dynamics of oligomerization, in particular how specific residues within Aβ control the process. To achieve this goal, here we have executed a strategy we term scanning PICUP that employs Tyr in a classical scanning amino acid substitution paradigm.

The use of Tyr, which is highly reactive in the photochemical cross-linking reaction on which PICUP is based, allowed us to simultaneously probe the effects of alteration of specific amino acid side chains on Aβ conformational dynamics and to determine how side-chain modifications affected peptide oligomerization. We note that the results thus obtained depend on the local environment of the Tyr residue within the Aβ monomer (*e.g.* its solvent accessibility) and on the oligomerization state of this monomer. The data thus reflect the sum of these phenomena. His and Met also may function in the PICUP chemistry, but their reactivity is substantially lower than that of Tyr (58), and thus the data discussed here reflect the activity of the substituted Tyr.

Qualitative analysis of the results of the CD studies of the Aβ40 and Aβ42 families of peptides comprising wild type and Tyr-substituted homologues showed that each family underwent an $RC \rightarrow \alpha/\beta \rightarrow \beta$ transition, as has been observed in prior studies (39, 53). However, detailed analysis of the results revealed substitution-dependent alterations in folding kinetics and conformer complexity. For each peptide family, the Tyr[1]-substituted homologue folded slowest, as assessed by determination of the midpoint of the secondary structure transition from $RC \rightarrow \beta$-sheet. This type of divergence from the dynamics of the wild type peptide also was observed in PICUP studies of oligomerization and EM studies of fibril formation. The oligomer frequency distribution of the substituted peptide was distinct, with an unusual doublet band apparent in SDS gels of the cross-linked population. It is significant that the Tyr[1] substitution in Aβ42 also produced an unusual oligomer distribution, one qualitatively similar to that seen in Aβ40, because this datum suggests that the effects of this substitution on the conformational dynamics of the peptide dominate those linked to the presence of Ile[41] and Ala[42].

In analyzing SDS-PAGE data such as those discussed above, one generally infers from the $M_r$ of a particular band that it includes *n*-order oligomers, where $n = M_r/MW_{monomer}$. However, this inference is valid only if the electrophoretic behavior of the analyte is ideal. We did not assume ideal behavior and therefore sought to formally determine the $M_r$ of a number of the bands. In doing so, we found that putative [Tyr[1]]Aβ40 monomers, dimers, and trimers yielded mass spectra consistent

with our order calculation. However, the putative tetramers and pentamers did not. Mass spectrometrically determined molecular weights for bands 4 and 5 were consistent with the masses of tetramers and pentamers, respectively, yet calculation of their $M_r$ values determined electrophoretically suggested they contained trimers and tetramers, respectively. These oligomers thus migrated anomalously. First principles suggest that the anomalously low $M_r$ was due to oligomer compaction. Direct experimental evidence for Aβ oligomer compaction has been obtained previously in studies of Aβ40, Aβ42, and homologues thereof (59, 60).

Aβ assembly involves intramolecular (within monomer) and intermolecular (within oligomers) interactions. Prior experimental and computational studies have revealed that important interaction sites controlling Aβ fibril formation exist within and adjacent to the central hydrophobic cluster (CHC; Leu[17]–Ala[21]) and the C terminus (48, 61–64). This knowledge has led naturally to the design of potential therapeutic agents targeting these sites, *e.g.* KLVFF-like peptide inhibitors (for a review, see Ref. 65) and inhibitors targeting the Aβ C terminus (66, 67). The ability of a single amino acid substitution at the N terminus (Tyr[1]) to alter the oligomer frequency distribution and the assembly kinetics suggests that the N terminus is not a benign peptide sub-region uninvolved in peptide assembly, as might be inferred from studies of fibril structure (68). It may be argued instead that the contribution of this region in the wild type peptide to the overall assembly energetics is significant but differs in magnitude from the contributions of the CHC and C terminus. Does this mean that therapeutic attention to this region is unwarranted? We would argue the contrary, namely that if the inhibitory effects of the Tyr[1] substitution can be amplified through selection of an appropriate small molecule inhibitor, then new and potentially efficacious assembly inhibitors may be discovered.

In addition to the CD experiments revealing effects of substitutions on folding kinetics, insights into the complexity of the conformational space of Aβ were obtained. The lack of a precise isodichroic point in CD spectra from the Aβ40 family shows that peptide assembly is not a simple two-state process (69, 70). However, we note that the spectra produced by the Tyr[40][Aβ40] peptide did converge, albeit imprecisely, near a specific point. This convergence does suggest a decrease in the conformational complexity of the system, as is clearly observed in the spectra of Aβ42, which display an isodichroic point. The Tyr[40] substitution in Aβ40 thus produces a secondary structure dynamics more akin to that seen in Aβ42. Consistent with this conclusion is the fact that the Tyr[40] substitution in Aβ40 substantially extended the highest order of oligomers observed in the PICUP experiments. For Aβ42, its conformational dynamics certainly must correlate with the increased hydrophobic surface of the peptide C terminus, which in turn may affect the stability of a C-terminal hinge (71) or turn (72) and the interactions of the C terminus with other regions of the peptide monomer, including the CHC. Because Aβ40 lacks two C-terminal residues and has not been found to form a turn in this region (72), our data suggest that the Tyr substitution in Aβ40 facilitates structural organization of the peptide monomer through interactions of the C terminus with the CHC. These interac-

tions may stabilize the monomer, restricting its exploration of conformational space and accounting for the quasi-isosbestic point in the CD spectra, an observation suggestive of the absence of intermediates in the conformational conversion process. We note, however, that the structural stabilization imparted on the Aβ40 peptide by the substitution of Tyr[40] does not result in an Aβ42-like oligomer distribution. An Aβ40-like oligomer distribution is maintained.

Our results elucidate the surprisingly complex structural dynamics of the relatively small Aβ peptide and how peptide segment-specific interactions may control the dynamics. A key determinant of how these interactions occur is the location of hinge or turn regions in the peptide. Evidence exists for turns in the Val[24]–Lys[28] region of Aβ in fibrils (for a recent review see Ref. 68) and in the Aβ monomer (72, 73), at the C terminus of Aβ42 (71, 72), at Glu[22]–Asp[23] in Aβ42 (74), and at other sites (62, 75, 76). Such turns bring regions relatively distant in the primary structure into proximity. For example, the turn at Gly[25]–Asn[27] would induce contacts between the CHC and C terminus, as well as among residues immediately adjacent to the turn itself. In the PICUP experiments reported here, we observed increased frequencies of higher order oligomers formed by the peptides in which the Tyr was substituted at Ala[30], Val[40], or Ala[42]. A reasonable explanation for these data is the effect of increased hydrophobicity of the substituted Tyr residue relative to the Ala and Val residues replaced. This would increase the stability of conformers in which hydrophobic side-chain packing occurred, as for example among residues forming the C-terminal turn or residues at the interface between the CHC and C-terminal peptide regions. This explanation also provides a mechanistic rationale for the increased oligomerization potential of the N-terminally substituted peptides, in which Tyr replaced Asp. This substitution produces a more hydrophobic N terminus, the increased solvophobic nature of which would favor intramolecular interactions with the apolar CHC (62). It is interesting in this regard that the N-terminal dipeptide substitution Glu-Val, which also increases the hydrophobicity of this peptide segment, facilitates protofibril formation (77).

In conclusion, one working hypothesis supported by our data is that Aβ conformational dynamics and assembly is a *competition* among interacting regions. For example, the ability of the extreme C terminus of Aβ42 to form a stable turn- or hinge-like structure creates a hydrophobic surface that can interact with the CHC to stabilize assembly-competent conformers. Because it lacks Ile[41] and Ala[42], Aβ40 cannot do so, yet the simple substitution of the Aβ40 C-terminal Val with Tyr does create a much more "Aβ42-like" peptide. The altered C terminus now "wins" the competition with the N terminus, an outcome observed *in silico* (62). The effect of Tyr substitution of Asp[1] is mechanistically similar. The substitution increases the stability of N terminus-CHC interactions, a result consistent with the observed compaction of the Tyr[1]-substituted peptides observed in SDS-PAGE. In this case, the N terminus competes more effectively with the C terminus. This mechanism suggests that rational targeting of specific Aβ subregions could be an effective therapeutic strategy. For example, agents could be designed to block C terminus-CHC interactions by binding to either or both subregions. Alternatively, agents that enhanced this interaction might facilitate fibril formation, which increasing evidence suggests may be protective (78). In fact, recent work has shown that C-terminal fragments of Aβ, when mixed with the full-length peptide, coaggregate and block the neurotoxic activity of the free peptide (78). Agents that bound to the N terminus and facilitated its binding to the CHC also could block formation of toxic assemblies.

## REFERENCES

1. Hebert, L. E., Scherr, P. A., Bienias, J. L., Bennett, D. A., and Evans, D. A. (2003) *Arch. Neurol.* **60,** 1119–1122
2. Brookmeyer, R., Johnson, E., Ziegler-Graham, K., and Arrighi, H. M. (2007) *Alzheimers Dement.* **3,** 186–191
3. Kirkitadze, M. D., Bitan, G., and Teplow, D. B. (2002) *J. Neurosci. Res.* **69,** 567–577
4. Klein, W. L., Stine, W. B., Jr., and Teplow, D. B. (2004) *Neurobiol. Aging* **25,** 569–580
5. Klyubin, I., Walsh, D. M., Cullen, W. K., Fadeeva, J. V., Anwyl, R., Selkoe, D. J., and Rowan, M. J. (2004) *Eur. J. Neurosci.* **19,** 2839–2846
6. Hardy, J., and Selkoe, D. J. (2002) *Science* **297,** 353–356
7. Klein, W. L., Krafft, G. A., and Finch, C. E. (2001) *Trends Neurosci.* **24,** 219–224
8. Small, D. H. (1998) *Amyloid* **5,** 301–304
9. Haass, C., and Steiner, H. (2001) *Nat. Neurosci.* **4,** 859–860
10. Shankar, G. M., Bloodgood, B. L., Townsend, M., Walsh, D. M., Selkoe, D. J., and Sabatini, B. L. (2007) *J. Neurosci.* **27,** 2866–2875
11. McLaurin, J., Kierstead, M. E., Brown, M. E., Hawkes, C. A., Lambermon, M. H., Phinney, A. L., Darabie, A. A., Cousins, J. E., French, J. E., Lan, M. F., Chen, F., Wong, S. S., Mount, H. T., Fraser, P. E., Westaway, D., and St George-Hyslop, P. (2006) *Nat. Med.* **12,** 801–808
12. Cheng, I. H., Scearce-Levie, K., Legleiter, J., Palop, J. J., Gerstein, H., Bien-Ly, N., Puoliväli, J., Lesné, S., Ashe, K. H., Muchowski, P. J., and Mucke, L. (2007) *J. Biol. Chem.* **282,** 23818–23828
13. Walsh, D. M., Klyubin, I., Fadeeva, J. V., Cullen, W. K., Anwyl, R., Wolfe, M. S., Rowan, M. J., and Selkoe, D. J. (2002) *Nature* **416,** 535–539
14. Oda, T., Wals, P., Osterburg, H. H., Johnson, S. A., Pasinetti, G. M., Morgan, T. E., Rozovsky, I., Stine, W. B., Snyder, S. W., Holzman, T. F., Krafft, G. A., and Finch, C. E. (1995) *Exp. Neurol.* **136,** 22–31
15. Lambert, M. P., Barlow, A. K., Chromy, B. A., Edwards, C., Freed, R., Liosatos, M., Morgan, T. E., Rozovsky, I., Trommer, B., Viola, K. L., Wals, P., Zhang, C., Finch, C. E., Krafft, G. A., and Klein, W. L. (1998) *Proc. Natl. Acad. Sci. U.S.A.* **95,** 6448–6453
16. Hartley, D. M., Walsh, D. M., Ye, C. P., Diehl, T., Vasquez, S., Vassilev, P. M., Teplow, D. B., and Selkoe, D. J. (1999) *J. Neurosci.* **19,** 8876–8884
17. Chen, Q. S., Kagan, B. L., Hirakura, Y., and Xie, C. W. (2000) *J. Neurosci. Res.* **60,** 65–72
18. Nalbantoglu, J., Tirado-Santiago, G., Lahsaïni, A., Poirier, J., Goncalves, O., Verge, G., Momoli, F., Welner, S. A., Massicotte, G., Julien, J. P., and Shapiro, M. L. (1997) *Nature* **387,** 500–505
19. Rowan, M. J., Klyubin, I., Cullen, W. K., and Anwyl, R. (2003) *Philos. Trans. R. Soc. Lond. B Biol. Sci.* **358,** 821–828
20. Westerman, M. A., Cooper-Blacketer, D., Mariash, A., Kotilinek, L., Kawarabayashi, T., Younkin, L. H., Carlson, G. A., Younkin, S. G., and Ashe, K. H. (2002) *J. Neurosci.* **22,** 1858–1867
21. Dahlgren, K. N., Manelli, A. M., Stine, W. B., Jr., Baker, L. K., Krafft, G. A., and LaDu, M. J. (2002) *J. Biol. Chem.* **277,** 32046–32053
22. Wang, H. W., Pasternak, J. F., Kuo, H., Ristic, H., Lambert, M. P., Chromy, B., Viola, K. L., Klein, W. L., Stine, W. B., Krafft, G. A., and Trommer, B. L.

(2002) *Brain Res.* **924,** 133–140

23. Cleary, J. P., Walsh, D. M., Hofmeister, J. J., Shankar, G. M., Kuskowski, M. A., Selkoe, D. J., and Ashe, K. H. (2005) *Nat. Neurosci.* **8,** 79–84

24. De Felice, F. G., Vieira, M. N., Saraiva, L. M., Figueroa-Villar, J. D., Garcia-Abreu, J., Liu, R., Chang, L., Klein, W. L., and Ferreira, S. T. (2004) *FASEB J.* **18,** 1366–1372

25. Walsh, D. M., Townsend, M., Podlisny, M. B., Shankar, G. M., Fadeeva, J. V., El Agnaf, O., Hartley, D. M., and Selkoe, D. J. (2005) *J. Neurosci.* **25,** 2455–2462

26. Head, E., Pop, V., Vasilevko, V., Hill, M., Saing, T., Sarsoza, F., Nistor, M., Christie, L. A., Milton, S., Glabe, C., Barrett, E., and Cribbs, D. (2008) *J. Neurosci.* **28,** 3555–3566

27. Kelly, B. L., and Ferreira, A. (2006) *J. Biol. Chem.* **281,** 28079–28089

28. White, J. A., Manelli, A. M., Holmberg, K. H., Van Eldik, L. J., and Ladu, M. J. (2005) *Neurobiol. Dis.* **18,** 459–465

29. Demuro, A., Mina, E., Kayed, R., Milton, S. C., Parker, I., and Glabe, C. G. (2005) *J. Biol. Chem.* **280,** 17294–17300

30. Chong, Y. H., Shin, Y. J., Lee, E. O., Kayed, R., Glabe, C. G., and Tenner, A. J. (2006) *J. Biol. Chem.* **281,** 20315–20325

31. Deshpande, A., Mina, E., Glabe, C., and Busciglio, J. (2006) *J. Neurosci.* **26,** 6011–6018

32. Lesné, S., Koh, M. T., Kotilinek, L., Kayed, R., Glabe, C. G., Yang, A., Gallagher, M., and Ashe, K. H. (2006) *Nature* **440,** 352–357

33. Townsend, M., Shankar, G. M., Mehta, T., Walsh, D. M., and Selkoe, D. J. (2006) *J. Physiol.* **572,** 477–492

34. Iwata, N., Tsubuki, S., Takaki, Y., Watanabe, K., Sekiguchi, M., Hosoki, E., Kawashima-Morishima, M., Lee, H. J., Hama, E., Sekine-Aizawa, Y., and Saido, T. C. (2000) *Nat. Med.* **6,** 143–150

35. Huang, S. M., Mouri, A., Kokubo, H., Nakajima, R., Suemoto, T., Higuchi, M., Staufenbiel, M., Noda, Y., Yamaguchi, H., Nabeshima, T., Saido, T. C., and Iwata, N. (2006) *J. Biol. Chem.* **281,** 17941–17951

36. Teplow, D. B. (2006) *Methods Enzymol.* **413,** 20–33

37. Bitan, G. (2006) *Methods Enzymol.* **413,** 217–236

38. Bitan, G., and Teplow, D. B. (2004) *Acc. Chem. Res.* **37,** 357–364

39. Maji, S. K., Amsden, J. J., Rothschild, K. J., Condron, M. M., and Teplow, D. B. (2005) *Biochemistry* **44,** 13365–13376

40. Fancy, D. A., Denison, C., Kim, K., Xie, Y., Holdeman, T., Amini, F., and Kodadek, T. (2000) *Chem. Biol.* **7,** 697–708

41. Walsh, D. M., Lomakin, A., Benedek, G. B., Condron, M. M., and Teplow, D. B. (1997) *J. Biol. Chem.* **272,** 22364–22372

42. Fezoui, Y., Hartley, D. M., Harper, J. D., Khurana, R., Walsh, D. M., Condron, M. M., Selkoe, D. J., Lansbury, P. T., Fink, A. L., and Teplow, D. B. (2000) *Amyloid Int. J. Exp. Clin. Invest.* **7,** 166–178

43. Jao, S. C., Ma, K., Talafous, J., Orlando, R., and Zagorski, M. G. (1997) *Amyloid Int. J. Exp. Clin. Invest.* **4,** 240–252

44. Zagorski, M. G., Yang, J., Shao, H., Ma, K., Zeng, H., and Hong, A. (1999) *Methods Enzymol.* **309,** 189–204

45. Stine, W. B., Jr., Dahlgren, K. N., Krafft, G. A., and LaDu, M. J. (2003) *J. Biol. Chem.* **278,** 11612–11622

46. LeVine, H., 3rd (2004) *Anal. Biochem.* **335,** 81–90

47. Walsh, D. M., Hartley, D. M., Kusumoto, Y., Fezoui, Y., Condron, M. M., Lomakin, A., Benedek, G. B., Selkoe, D. J., and Teplow, D. B. (1999) *J. Biol. Chem.* **274,** 25945–25952

48. Bitan, G., Kirkitadze, M. D., Lomakin, A., Vollers, S. S., Benedek, G. B., and Teplow, D. B. (2003) *Proc. Natl. Acad. Sci. U.S.A.* **100,** 330–335

49. Bitan, G., Lomakin, A., and Teplow, D. B. (2001) *J. Biol. Chem.* **276,** 35176–35184

50. Ezra, D., Castillo, U. F., Strobel, G. A., Hess, W. M., Porter, H., Jensen, J. B., Condron, M. A., Teplow, D. B., Sears, J., Maranta, M., Hunter, M., Weber, B., and Yaver, D. (2004) *Microbiology* **150,** 785–793

51. Fradinger, E. A., Maji, S., Lazo, N. D., and Teplow, D. B. (2005) in *Amyloid Precursor Protein: A Practical Approach* (Xia, W., and Xu, H., eds) pp. 83–110, CRC Press, Inc., Boca Raton, FL

52. Sreerama, N., and Woody, R. W. (2000) *Anal. Biochem.* **287,** 252–260

53. Kirkitadze, M. D., Condron, M. M., and Teplow, D. B. (2001) *J. Mol. Biol.* **312,** 1103–1119

54. Castellanos-Serra, L., Proenza, W., Huerta, V., Moritz, R. L., and Simpson, R. J. (1999) *Electrophoresis* **20,** 732–737

55. Walsh, D. M., and Selkoe, D. J. (2004) *Protein Pept. Lett.* **11,** 213–228

56. Haass, C., and Selkoe, D. J. (2007) *Nat. Rev. Mol. Cell Biol.* **8,** 101–112

57. Walsh, D. M., and Selkoe, D. J. (2007) *J. Neurochem.* **101,** 1172–1184

58. Kotzyba-Hibert, F., Kapfer, I., and Goeldner, M. (1995) *Angew. Chem. Int. Ed. Engl.* **34,** 1296–1312

59. Bernstein, S. L., Wyttenbach, T., Baumketner, A., Shea, J. E., Bitan, G., Teplow, D. B., and Bowers, M. T. (2005) *J. Am. Chem. Soc.* **127,** 2075–2084

60. Baumketner, A., Bernstein, S. L., Wyttenbach, T., Bitan, G., Teplow, D. B., Bowers, M. T., and Shea, J. E. (2006) *Protein Sci.* **15,** 420–428

61. Morimoto, A., Irie, K., Murakami, K., Masuda, Y., Ohigashi, H., Nagao, M., Fukuda, H., Shimizu, T., and Shirasawa, T. (2004) *J. Biol. Chem.* **279,** 52781–52788

62. Urbanc, B., Cruz, L., Yun, S., Buldyrev, S. V., Bitan, G., Teplow, D. B., and Stanley, H. E. (2004) *Proc. Natl. Acad. Sci. U.S.A.* **101,** 17345–17350

63. Hilbich, C., Kisters-Woike, B., Reed, J., Masters, C. L., and Beyreuther, K. (1992) *J. Mol. Biol.* **228,** 460–473

64. Wood, S. J., Wetzel, R., Martin, J. D., and Hurle, M. R. (1995) *Biochemistry* **34,** 724–730

65. Mason, J. M., Kokkoni, N., Stott, K., and Doig, A. J. (2003) *Curr. Opin. Struct. Biol.* **13,** 526–532

66. Hetényi, C., Szabó, Z., Klement, E., Datki, Z., Körtvélyesi, T., Zarándi, M., and Penke, B. (2002) *Biochem. Biophys. Res. Commun.* **292,** 931–936

67. Szegedi, V., Fülöp, L., Farkas, T., Rózsa, E., Robotka, H., Kis, Z., Penke, Z., Horváth, S., Molnár, Z., Datki, Z., Soós, K., Toldi, J., Budai, D., Zarándi, M., and Penke, B. (2005) *Neurobiol. Dis.* **18,** 499–508

68. Tycko, R. (2006) *Q. Rev. Biophys.* **39,** 1–55

69. Chellgren, B. W., Miller, A. F., and Creamer, T. P. (2006) *J. Mol. Biol.* **361,** 362–371

70. Fändrich, M., Forge, V., Buder, K., Kittler, M., Dobson, C. M., and Diekmann, S. (2003) *Proc. Natl. Acad. Sci. U.S.A.* **100,** 15463–15468

71. Lansbury, P. T., Jr., Costa, P. R., Griffiths, J. M., Simon, E. J., Auger, M., Halverson, K. J., Kocisko, D. A., Hendsch, Z. S., Ashburn, T. T., Spencer, R. G., *et al.* (1995) *Nat. Struct. Biol.* **2,** 990–998

72. Lazo, N. D., Grant, M. A., Condron, M. C., Rigby, A. C., and Teplow, D. B. (2005) *Protein Sci.* **14,** 1581–1596

73. Grant, M. A., Lazo, N. D., Lomakin, A., Condron, M. M., Arai, H., Yamin, G., Rigby, A. C., and Teplow, D. B. (2007) *Proc. Natl. Acad. Sci. U.S.A.* **104,** 16522–16527

74. Murakami, K., Irie, K., Ohigashi, H., Hara, H., Nagao, M., Shimizu, T., and Shirasawa, T. (2005) *J. Am. Chem. Soc.* **127,** 15168–15174

75. Williams, A. D., Portelius, E., Kheterpal, I., Guo, J. T., Cook, K. D., Xu, Y., and Wetzel, R. (2004) *J. Mol. Biol.* **335,** 833–842

76. Hilbich, C., Kisters-Woike, B., Reed, J., Masters, C. L., and Beyreuther, K. (1991) *J. Mol. Biol.* **218,** 149–163

77. Qahwash, I., Weiland, K. L., Lu, Y., Sarver, R. W., Kletzien, R. F., and Yan, R. (2003) *J. Biol. Chem.* **278,** 23187–23195

78. Fradinger, E. A., Monien, B. H., Urbanc, B., Lomakin, A., Tan, M., Li, H., Spring, S. M., Condron, M. M., Cruz, L., Xie, C. W., Benedek, G. B., and Bitan, G. (2008) *Proc. Natl. Acad. Sci. U.S.A.* **105,** 14175–14180